Evaluation of temperature and wind over Antarctica in a Regional Atmospheric Climate Model using 1 year of automatic weather station data and upper air observations

C. H. Reijmer
Institute for Marine and Atmospheric Research, Utrecht University, Utrecht, Netherlands

E. van Meijgaard
Royal Netherlands Meteorological Institute, De Bilt, Netherlands

M. R. van den Broeke
Institute for Marine and Atmospheric Research, Utrecht University, Utrecht, Netherlands

Received 15 July 2004; revised 8 October 2004; accepted 28 December 2004; published 18 February 2005.

[1] The Regional Atmospheric Climate Model version 2 (RACMO2/ANT) is used to simulate the Antarctic atmosphere for the year 1998. The parameterizations of the physical processes in the model are taken from the European Centre for Medium-Range Weather Forecasts (ECMWF) global model and adapted to better represent the specific conditions over the Antarctic continent. The snow albedo was increased by decreasing the rate of albedo change as a function of temperature. This results in a decrease, and an improvement, in near-surface air temperatures in summer, especially over the Antarctic plateau. The surface roughness length for momentum was decreased. This increases the wind speed over the total atmospheric column. As a result, wind speeds better correspond to measurements, especially near the surface and in high wind speed areas. Comparison with ECMWF 40-year reanalyses (ERA40) data show that RACMO2/ANT better reproduces the near-surface conditions in terms of temperature and wind speed mainly due to the changes made to the physics description. Away from the surface, ERA40 better corresponds to observations due to the inclusion of the observed profiles in the reanalyses.

Citation: Reijmer, C. H., E. van Meijgaard, and M. R. van den Broeke (2005), Evaluation of temperature and wind over Antarctica in a Regional Atmospheric Climate Model using 1 year of automatic weather station data and upper air observations, *J. Geophys. Res.*, *110*, D04103, doi:10.1029/2004JD005234.

1. Introduction

[2] In the last few decades considerable advances have been made in numerical modelling of the Antarctic atmosphere. Several factors have contributed to this progress, e.g, extension of the observational network [*Reijmer and Oerlemans*, 2002; *Reusch and Alley*, 2004], dedicated field campaigns [*Bintanja*, 2000; *Cassano et al.*, 2001; *Van As et al.*, 2005], evaluations of atmospheric models [*King and Turner*, 1997; *King et al.*, 2001; *Van Lipzig et al.*, 1999; *Turner et al.*, 1999] and increasing computational power. The models improved our understanding of the physical processes of the Antarctic climate system [*Van den Broeke et al.*, 2002; *Van Lipzig et al.*, 2002] and its link to global climate [*Cullather et al.*, 1996; *Van den Broeke*, 2000].

[3] With the increase of our knowledge, the demand on model performance increased as well, both in terms of physical parameterizations and in spatial resolution. To accommodate the demand for higher resolution and still limit the computational costs, limited area models (LAMs) are more and more used for Antarctic climate research [*Walsh and McGregor*, 1996; *Van den Broeke et al.*, 2002; *Van Lipzig et al.*, 2002; *Guo et al.*, 2003; *Bromwich et al.*, 2004]. An additional advantage of LAMs over global models is that LAMs can be adapted to the specific conditions of the Antarctic continent, which is more difficult with global models. A disadvantage is that a LAM needs a forcing at the boundaries of its domain. This forcing is provided by output of global models. Unfortunately, this makes studies of climate sensitivity with LAMs difficult because feedback to global climate is not possible. However, the relatively high resolutions possible with LAMs and the still limited amount of observations made over the Antarctic continent make LAMs potentially very valuable in studying recent Antarctic climate variations.

[4] Recently, the European Centre for Medium-Range Weather Forecasts (ECMWF) completed a reanalyses project covering 45 years (1957–2002, ERA40). The model

0148-0227/05/2004JD005234$09.00

used for the reanalyses was improved considerably compared to the one used for the 15-year reanalyses the ECMWF carried out in 1994 (ERA15) [*Gibson et al.*, 1997]. The main improvements for the Antarctic continent are a change in model orography, a change in stability functions preventing the lowest model layer to decouple from the rest of the troposphere under very stable conditions [*Viterbo et al.*, 1999] and the description of ice shelves as grounded ice instead of sea ice [*Genthon and Braun*, 1995]. Because the NCEP-NCAR reanalysis, which is similar in length as ERA40, has known deficiencies in representation of the Antarctic atmosphere [*Cullather et al.*, 1998; *Hines et al.*, 2000], the new ERA40 data set is a valuable additional tool for (Antarctica) climate research. However, although the resolution of ERA40 (spectral resolution of T159, corresponding to $\sim$1.1° spatial resolution, and 60 vertical levels) is better than the NCEP-NCAR resolution (T62, $\sim$2.9°, 28 levels) and the ERA15 resolution (T106, $\sim$1.7°, 31 levels), for a reasonable representation of the Antarctic topography a higher horizontal resolution is desirable. Therefore, a potentially valuable combination would be to use the ERA40 data set as forcing for a LAM.

[5] The results presented here are part of a project that aims at modeling the Antarctic climate using a limited area model with the ERA40 output as forcing at its lateral boundaries. The project is a continuation of the Antarctic climate research with a Regional Atmospheric Climate Model, RACMO1/ANT presented by *Van Lipzig et al.* [1999]. We use a newly developed model with a more up to date dynamics and physics package which also incorporates improvements based on the findings of *Van Lipzig et al.* [1999]. For example, the formulation for the roughness length for heat and moisture is changed to prevent too high sublimation rates as found by *Van Lipzig et al.* [2002], and the albedo formulation is changed to reduce the small warm bias over the Antarctic plateau in summer [*Van Lipzig*, 1999].

[6] Prerequisite for further use of the data is an evaluation of the model results, which is presented in this paper. In section 2 we describe the model and the changes we made to the physics description. Section 3 presents results of experiments with the model changes and section 4 presents a comparison of the results with ERA40 data and observations. We conclude with a summary and a discussion of the results.

2. Model Description and Data

2.1. Model Setup

[7] We use the Regional Atmospheric Climate Model version 2 (RACMO2) of the Royal Netherlands Meteorological Institute (KNMI). RACMO2 is in fact a combination of two models. The formulation of the dynamical processes is adopted from the High Resolution Limited Area Model (HIRLAM, version 5.0.6 [*Undén et al.*, 2002]). The parameterizations of the physical processes are taken from the ECMWF model (cycle CY23R4 [*White*, 2001]). We made some adjustments to the model formulation to better represent the conditions over Antarctica. The main features of the model and the adjustments to the physics are described in this section.

[8] Figure 1 shows the horizontal model grid of RACMO2 over Antarctica. The horizontal resolution is $\sim$55 km and the area covered by the 122 $\times$ 134 model grid points covers the Antarctic continent and a large part of the Southern Ocean. In the vertical the model has 40 hybrid-levels, which are terrain following (σ) levels close to the surface and pressure levels at higher altitudes. The lowest 32 model levels are in the troposphere, the lowest 10 levels are in the lowest kilometer and the lowest level is at $\sim$10 m above the surface. The model is initialized once and forced every six hours at the lateral boundaries and at the sea surface by ECMWF operational analyses. The inner part of the model is allowed to evolve freely. In the lateral boundary zone of 8 points wide the prognostic variables are relaxed towards the ECMWF analyses (Figure 1). The model time step is 720 s, which is possible due to a semi-lagrangian time scheme.

[9] The model surface geopotential is based on the Radarsat Antarctic Mapping Project Digital Elevation Model (RAMP 2002, http:/nsidc.org/data/nsidc-0082.html). This topography includes the ice shelves. The RAMP topography is based on a variety of sources to provide the most accurate, up to date and consistent map of Antarctica. Sources are, e.g., satellite radar altimetry data, the Antarctic Digital Database and U.S. Geological Survey topographic maps. The land-sea mask is based on the RAMP topography using a threshold elevation of 25 m. The sea ice mask is based on the ECMWF analyses of the sea surface temperature using a threshold of 271.46 K, the freezing point of sea water. No fractional sea ice cover is considered.

2.2. Model Physics

[10] An extensive description of the model physics can be found in *White* [2001]. Here, we describe the main features.

[11] To calculate the long wave radiative fluxes a modified version of the Rapid Radiation Transfer Model (RRTM) is used [*Mlawer et al.*, 1997]. In this model the absorption coefficients are mapped to a space of probability density functions using the correlated-k method, making it possible to describe the long wave radiative fluxes in 9 spectral intervals with a total of 140 subintervals. For the short wave radiative fluxes a two-stream formulation is used in which the fluxes are integrated over two spectral bands [*Fouquart and Bonnel*, 1980]. The model includes scattering processes and molecular absorption. The surface reflectance or albedo formulation is discussed in section 2.3.1.

[12] The surface turbulent fluxes are calculated from Monin-Obukhov similarity theory using transfer coefficients based on the *Louis* [1979] expressions. An effective roughness length is introduced for momentum and heat to account for the effect of subgrid-scale orographic variations on the grid resolved flow. The roughness length formulation is discussed in section 2.3.2. Above the surface layer a first order closure scheme is used to parameterize the turbulent exchange. The exchange coefficients depend on the stability regime and on the vertical location above the surface. The schemes used for the different stability regimes are nonlocal diffusion from *Troen and Mahrt* [1986], local diffusion dependent on the Richardson number or local diffusion with Monin-Obukhov functions.

[13] Orographic drag is described as a combination of lower-tropospheric drag and vertical profiles of drag. The former is created by orography assumed to intersect model levels. The latter is related to vertically propagating gravity

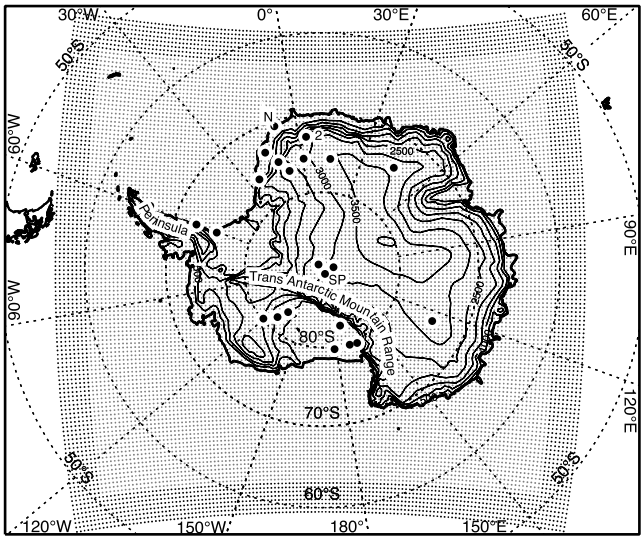

Figure 1. The RACMO2/ANT model grid. The small black dots indicate the relaxation zone where model prognostic variables are relaxed towards ECMWF analyses. Contour lines indicate surface height. The contour interval is 500 m. Large black dots denote the locations of the (automatic) weather stations. N is Neumayer station, SP is South Pole station, 2 is AWS 2.

waves that are absorbed and reflected by a stably stratified flow over the subgrid-scale orography. A grid point region is described by the subgrid standard deviation, anisotropy, slope and geographical orientation of the RAMP orography.

[14] Cumulus convection is described by a bulk mass flux scheme based on the scheme of *Tiedke* [1989]. The scheme considers deep, midlevel and shallow convection. Clouds are represented by a single pair of entraining/detraining plumes describing updraught and downdraught processes. Clouds and large-scale precipitation processes are described by prognostic equations for cloud liquid water, cloud ice and cloud fraction, and diagnostic equations for precipitation.

[15] The land surface processes are described using the Tiled ECMWF Scheme for Surface Exchanges over Land (TESSEL [*Viterbo et al.*, 1999]). A grid box is either a 100% water, sea ice or land grid box. The land grid boxes can be tiled in 6 different fractions of land cover types among which snow covered bare soil. All snow surfaces on land are described as a single layer of snow on top of the soil. The heat diffusion equation is solved for the four soil layers with no heat flux through the lowest layer at 2.6 m depth. The surface temperature of snow or soil is described using a skin temperature formulation based on an infinitely thin surface layer without heat capacity. The description of land ice is discussed in section 2.3.3. Sea ice is described using a four-layer model with a skin temperature formulation at the surface and the freezing temperature of sea water at the bottom. The Antarctic sea ice thickness is set to a constant value of 1.5 m.

2.3. Physics Adjustments

[16] Experiments with other models [*Van Lipzig et al.*, 1999; *Cassano et al.*, 2001; *King et al.*, 2001; *Guo et al.*, 2003; *Reijmer et al.*, 2004] have shown that the physics of atmospheric models need adjustments before optimal performance is achieved over Antarctica. The problems with the models are mainly related to the exceptionally stable boundary layer over Antarctica and the surface and subsurface characteristics. Here, we describe the changes we have made to the original ECMWF model physics formulation in RACMO2. They are summarized in Table 1. We will call the changed model henceforth RACMO2/ANT.

2.3.1. Snow Albedo

[17] The original calculation of the snow albedo over land is based on the method described by *Douville et al.* [1995]. The surface albedo ages at a constant rate after a snowfall event when the snow temperature (T_{sn}) is <0°C:

$$\alpha_{sn}(t+\Delta t) = \alpha_{sn}(t) - k_a \frac{\Delta t}{\tau_{day}} , \qquad (1)$$

and at an exponential rate when $T_{sn} \geq 0$°C:

$$\alpha_{sn}(t+\Delta t) = (\alpha_{sn}(t) - \alpha_{\min})\exp\left(-k_f \frac{\Delta t}{\tau_{day}}\right) + \alpha_{\min} . \qquad (2)$$

Here, α_{sn} is the snow albedo, k_a is a constant reduction rate (0.008), k_f is an exponential e-folding coefficient (0.24), τ_{day} is 86400 s, t is model time and Δt is the model time step in seconds. The snow albedo is 0.85 after a snowfall event and decreases to a lower limit ($\alpha_{\min}$) of 0.75 in ~12.5 days for $T_{sn} < 0$°C (Figure 2). This decrease of α_{sn} to its lower limit is too fast. The actual rate of albedo change depends on temperature and decreases with decreasing temperature [*Warren*, 1982].

[18] To reduce the rate of albedo change for $T_{sn} < 0$°C, the method described by *Van den Hurk and Viterbo* [2003] is implemented in RACMO2/ANT. In this method the albedo does not only depend on elapsed time since the snowfall event but also on T_{sn}:

$$\alpha_{sn}(t+\Delta t) = \alpha_{sn}(t) - k_a \frac{\Delta t}{\tau_{day}\left(1 + 0.1 * T_{sn}^4\right)} , \qquad (3)$$

where T_{sn} is in °C. Furthermore, $\alpha_{\min}$ is changed to 0.8. Figure 2 shows that using equation (3) the rate of albedo

Table 1. Description of the Model Experiments[a]

	ORI	CTL
z_{0m}	*White* [2001]	equation (4)
z_{0h}	*White* [2001]	equation (5)
$\alpha_{\min}$ snow	0.75	0.8
$\alpha_{\min}$ sea ice	0.50	0.6
ρ_{ini}, kg m^{-3}	225	350
$\rho_{\max}$, kg m^{-3}	300	350
T_{skin}	T_{soil}	$T_{e,sn}$
T_{sn}	T_{soil}	$T_{e,sn}$
dz_{sn}, m	1	0.1
dz_{fresh}, mm w.e. hr^{-1}	1	1/3
$\alpha(t+\Delta t)$	equation (1)	equation (3)
α_{si}	climate	equation (3)
snow model	no	yes

[a]Notes: z_{0m}, roughness length for momentum; z_{0h}, roughness length for heat; $\alpha_{\min}$, lower limit albedo; ρ_{ini}, initial snow density; $\rho_{\max}$, maximum snow density; T_{skin}, skin layer temperature; T_{sn}, snow layer temperature; T_{soil}, ECMWF soil temperature; $T_{e,sn}$, ECMWF snow layer temperature; dz_{sn}, thickness of the top snow layer for thermal calculations; dz_{fresh}, threshold flux of fresh snow for changes in the albedo; $\alpha(t+\Delta t)$, albedo change; α_{si}, sea ice albedo.

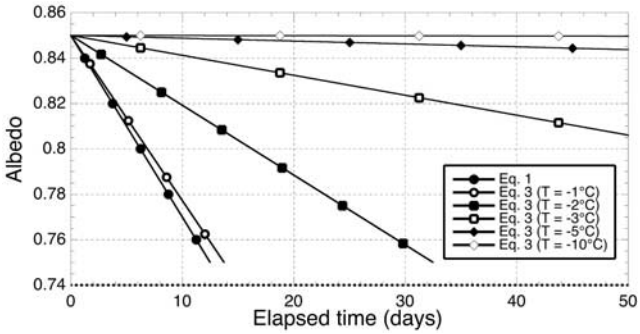

Figure 2. Albedo change after a snowfall event as a function of elapsed time since the event, assuming a constant temperature. See the text for the equations.

change decreases dramatically for temperatures below 0°C to almost no change for $T_{sn} < -10$°C.

[19] The original threshold of minimum amount of snowfall that changes the snow albedo to the value of freshly fallen snow had been set to 1 mm water equivalent per hour (w.e. hr^{-1}). Because of the low precipitation amounts over the Antarctic continent we changed this threshold to 0.33 mm w.e. hr^{-1}.

[20] The original sea ice albedo (α_{si}) parameterization is based on a climatology containing a seasonal cycle. In RACMO2/ANT we have changed that to the same formulation as used for snow covered land surfaces. The sea ice albedo is 0.85 after a snowfall event, and $\alpha_{\min}$ and α_{si} for freshly formed sea ice are both set to 0.6.

2.3.2. Roughness Lengths

[21] The original description of the model effective surface roughness length for momentum (z_{0m}) over land surfaces is based on vegetation maps that are corrected for urbanization and orography by applying the method described by *White* [2001], using the U.S. Navy data set. In RACMO2/ANT the resulting field is constrained using:

$$z_{0m} = 10^{-3} + \frac{\max\left[\left(z_{0m\,org} - z_{0m\,lvl}\right), 0\right]}{\left(100 - z_{0m\,lvl}\right)/z_{0m\,\max}} \ , \qquad (4)$$

where $z_{0m\ org}$ is the original roughness length. This limits z_{0m} to a maximum value ($z_{0m\ \max}$) of 1.0 m and for $z_{0m\ org}$ smaller than a threshold value $z_{0m\ lvl}$ of 5.0 m, z_{0m} is set to 10^{-3} m, which is the climatological value of z_{0m} of snow without the effect of orography taken into account. This value is still reasonably high when compared to observations over Antarctic snow surfaces which yield values of 4.0 10^{-6} m to 10^{-3} m [*King and Turner*, 1997]. Figure 3 presents the resulting field for z_{0m}. Compared to the original field (not shown) z_{0m} is reduced from maximum values of 100 m in mountainous areas to 1 m, and over flat terrain z_{0m} is a constant value of 10^{-3} m.

[22] The method described by *White* [2001] for the original model also produces a separate field for the roughness length for heat (z_{0h}). The roughness length for moisture (z_{0q}) is set equal to z_{0h}. However, the z_{0h} field determined this way exhibits a latitudinal dependency (not shown) and therefore, we have chosen to use the surface renewal model of *Andreas* [1987] to describe z_{0h} over snow and ice surfaces in RACMO2/ANT. This model was tested

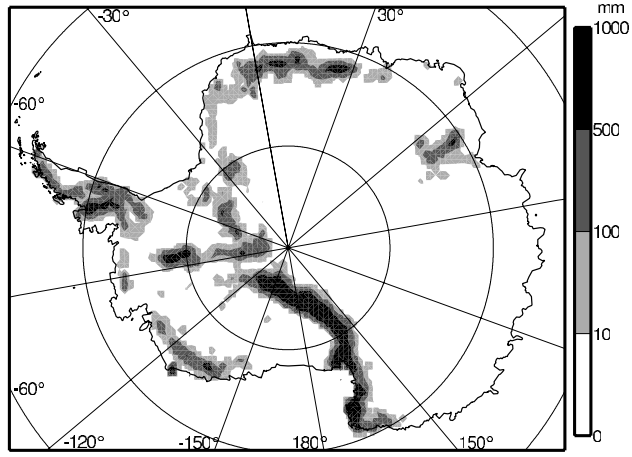

Figure 3. Surface roughness length for momentum (z_{0m}) based on the method described by *White* [2001] and modified by equation (4).

for different snow and ice surfaces by *Andreas* [2002] and tested for Antarctica in an atmospheric model by *Reijmer et al.* [2004]. The surface renewal model predicts $\ln(z_{0h}/z_{0m})$ as a function of the roughness Reynolds number (Re_*):

$$\ln\left(\frac{z_{0h}}{z_{0m}}\right) = a_1 + a_2\ \ln\left(Re_*\right) + a_3\ \ln\left(Re_*\right)^2 \ , \qquad (5)$$

$$Re_* = \frac{u_*\, z_{0m}}{\nu} \ . \qquad (6)$$

Here, $a1$, a_2 and a_3 are constants depending on Re_* (Table 2), u_* is the friction velocity and ν is the kinematic viscosity. The density dependency of ν is not taken into account, a constant value of $1.35\ 10^{-5}\ m^2\ s^{-1}$ is assumed. z_{0m} in equation (6) is set to a constant value of 10^{-3} m, neglecting the orographic component of z_{0m}. Application of equation (5) results in a dependency of z_{0h} on the near-surface wind speed through u_*. The roughness length for moisture is again assumed to be equal to z_{0h}. Equation (5) is applied to all snow and ice surfaces in the model, including sea ice, and is found to produce values similar to the original field.

2.3.3. Snow Model

[23] The original model formulation does not make a distinction between ice sheets and seasonal snow cover. Ice or snow on land is treated as one additional layer on top of the soil which is in thermal contact with the soil. The climatological depth of that layer is 10 m w.e. for the Antarctic ice sheet. The layer has an average temperature and density based on *Douville et al.* [1995]. Because a single snow layer of 10 m w.e. has a large thermal inertia, the depth for the thermal calculations is limited to 1 m of snow.

Table 2. Coefficients Used in Equation (5)[a]

	$Re_* \le 0.135$	$0.135 < Re_* < 2.5$	$2.5 \le Re_* \le 1000$
a_1	1.250	0.149	0.317
a_2	-	−0.550	−0.565
a_3	-	-	−0.183

[a]From *Andreas* [1987].

[24] The snow temperature depends on the energy flux at the surface and at the bottom of the layer, the depth of the snow layer and the volumetric heat capacity of snow ($(\rho C)_{sn}$). $(\rho C)_{sn}$ is density dependent:

$$(\rho C)_{sn} = (\rho C)_{ice} \frac{\rho_{sn}}{\rho_{ice}} , \quad (7)$$

where $(\rho C)_{ice}$ is the volumetric heat capacity of ice ($2.05\ 10^6$ J m^{-3} K^{-1}), ρ_{sn} is the density of the snow layer and ρ_{ice} is the ice density (920 kg m^{-3}). In case of melt all water runs off and refreezing of melt water in the snowpack is not accounted for. The heat flux from the snow layer to the underlying layer is determined by the temperature gradient between them, and the thermal conductivity of both layers. The thermal conductivity of snow (λ_{sn}) is density dependent:

$$\lambda_{sn} = \lambda_{ice} \times \left(\frac{\rho_{sn}}{\rho_{ice}} \right)^{1.88} , \quad (8)$$

where λ_{ice} is the ice thermal conductivity (2.2 W m^{-2}K^{-1}).

[25] Snow density varies between 100 kg m^{-3} (fresh snow) and 350 kg m^{-3} (ρ_{max}). The density increases exponentially in time due to aging of the snow:

$$\rho_{sn}(t + \Delta t) = (\rho_{sn}(t) - \rho_{max}) \exp\left(-k_f \frac{\Delta t}{\tau_{day}} \right) + \rho_{max} . \quad (9)$$

After a snowfall event ρ_{sn} is recalculated as a depth weighted average between the density of the old snow and fresh snow.

[26] To improve the thermal characteristics of the snow surface in RACMO2/ANT a four-layer snow model was added between the snow layer already present and the first soil layer. The description of the top snow layer remains the same except for the depth of the layer for thermal calculations, which is changed to 0.1 m snow. The thicknesses of the layers in the snow model are constant and set to 0.25 m, 0.75 m, 3.0 m and 6.0 m snow. The density of these layers is constant and set to typical Antarctic values of 350 kg m^{-3}, 400 kg m^{-3}, 450 kg m^{-3} and 500 kg m^{-3}, respectively. The heat transfer between the layers is described by

$$(\rho C)_{sn} \frac{\delta T_{sn}}{\delta t} = \frac{\delta}{\delta z} \left(\lambda_{sn} \frac{\delta T_{sn}}{\delta z} \right) , \quad (10)$$

where z is depth. The heat flux between the top snow layer and the first layer of the snow model depends on the temperature gradient between the two layers and the thermal conductivity of the layers. At the bottom of the snow model a zero heat flux to the soil is assumed. There is no melt or refreezing in the snow model. Due to the low temperatures on the Antarctic continent melt seldom occurs and from this we suppose this simplification in the snow model can be justified.

2.4. Experiments

[27] We used the model with full modified physics to carry out a model run (CTL) for the year 1998. The model prognostic fields (wind, temperature, specific humidity and surface pressure) are initialized on 1 January 1998 0:00 UTC using ECMWF operational analyses. The skin temperature and snow temperatures are initialized using the ECMWF snow temperature. To test the impact of the changes in the physics we carried out a run for 1998 in which we used the original ECMWF physics formulation (ORI). This run includes the unmodified field for z_{0m} and z_{0h}, and initialization of the skin and snow temperature using ECMWF soil temperatures (Table 1).

[28] In addition to the performance test, we compare RACMO2/ANT results with ERA40 for 1998. The ERA40 model is a global model with a spectral resolution of T159 ($\sim$1.1°) and a vertical resolution of 60 hybrid levels. Observations of atmospheric parameters are assimilated into the model using a 3D-variational technique resulting in the analyses used here for the model comparison.

2.5. Observations

[29] The model results are compared with observations, which are (automatic) weather station data from 15 stations of the United States Antarctic Program (USAP) [*Stearns et al.*, 1997], Neumayer station [*König-Langlo et al.*, 1998], Halley station, and 6 stations in Dronning Maud Land [*Reijmer and Oerlemans*, 2002] (Figure 1). Of these 23 stations 10, including Neumayer, are located on ice shelves, 2 are located in the escarpment region and 11, including South Pole (Clean Air station), are located on the Antarctic Plateau. Furthermore, balloon soundings at Neumayer and South Pole for January and July 1998 are used. Weather station data and balloon soundings of the USAP stations, Neumayer and Halley are available from the internet. The sites are http://uwamrc.ssec.wisc.edu/amrc/archiv.html, http://www.awi-bremerhaven.de/MET/Neumayer/met.html and http://www.antarctica.ac.uk/met/data.html, respectively. Note that the comparison with observations and especially vertical profiles is not unambiguous. Observations generally reflect local conditions and need not be representative for a grid box average as results from the model.

[30] Due to the limited horizontal resolution of the model, steep slopes are flattened out possibly resulting in inadequate values of elevation and slope at the model grid point closest to the station location. Therefore, the closest grid point with a reasonable correspondence in elevation and slope is chosen for the comparison with observations instead of the grid point closest to the observation site. The chosen grid points are within $\sim$80 km of the observation sites, and the model elevation at these points is within $\sim$50 m of the actual elevation. The slope is generally underestimated in the model, the steeper the actual slope the greater this effect. Temperatures and wind speeds are not corrected for the deviations in elevation and slope.

3. Results: Model Changes

3.1. Near-Surface Conditions

3.1.1. Wind Speed

[31] Table 3 presents temporal and continentally averaged near-surface wind speeds for January, July and the year 1998. It shows an increase in near-surface wind speed with about a factor two. Annual averaged wind speed increases from $\sim$3.7 m s^{-1} in ORI to $\sim$7.1 m s^{-1} in CTL. *Reijmer et al.* [2004] show that in their model a reduction in z_{0m} results

Table 3. Continentally Averaged Modeled 10-m Wind Speed (*WS*), Wind Speed at the Lowest Model Level (WS_{lvl}), Surface Temperature (T_0), 2-m Temperature (T_2), and Temperature at the Lowest Model Level (T_{lvl}) (at ~10 m Above the Surface)[a]

	T_0	T_2	T_{lvl}	*WS*	WS_{lvl}
	(K)			(m s^{-1})	
		January			
ORI	258.1	258.8	259.0	2.3	2.0
CTL	253.4	254.4	254.8	4.9	4.8
ERA40	259.0	258.5	260.0	4.0	4.0
		July			
ORI	224.4	227.7	228.7	4.2	3.8
CTL	223.9	227.5	228.3	7.8	7.6
ERA40	222.0	226.1	230.7	7.7	7.2
		1998			
ORI	238.2	240.3	241.0	3.7	3.2
CTL	235.3	237.9	238.5	7.1	6.9
ERA40	234.7	237.0	241.2	6.5	6.3

[a]Monthly averages for January and July 1998, and annual averages for 1998 are presented.

in an increase of the simulated wind speed. Therefore, an additional experiment in which only z_{0m} was changed compared to ORI was carried out (not shown). It confirmed that the reduction in wind speed is indeed mainly due to the reduction of z_{0m}. The basic effect of reducing z_{0m} is a reduction in the friction exerted by the surface on the atmospheric flow, resulting in an increase in near-surface wind speed that is largest in the areas where the reduction in z_{0m} is largest (Figures 3 and 4). These are also the areas where the surface slope is largest and the near-surface wind speed is highest. As a result, wind speeds increase over the whole continent when reducing z_{0m}. The wind speed increase is largest in winter when wind speeds are highest.

[32] Comparison with observations shows that the model generally overestimates the near-surface wind speed in low wind speed areas and underestimates it in high wind speed areas (Figure 5a). Over Antarctica, the near-surface wind field is largely determined by a semi-permanent katabatic flow. This katabatic flow is forced by cooling of the near-surface air over a sloping surface, which forces a down slope pressure gradient inducing a down slope gravitational flow [*Parish and Bromwich*, 1991]. The result is that errors in the orography of the model result in errors in the near-surface wind field. Owing to the limited horizontal resolution of the model, surface slopes are overestimated in flat areas and underestimated in areas with steep surface slopes. This explains, in combination with the presence of a very persistent katabatic flow over Antarctica, part of the difference between the modeled and observed wind speed.

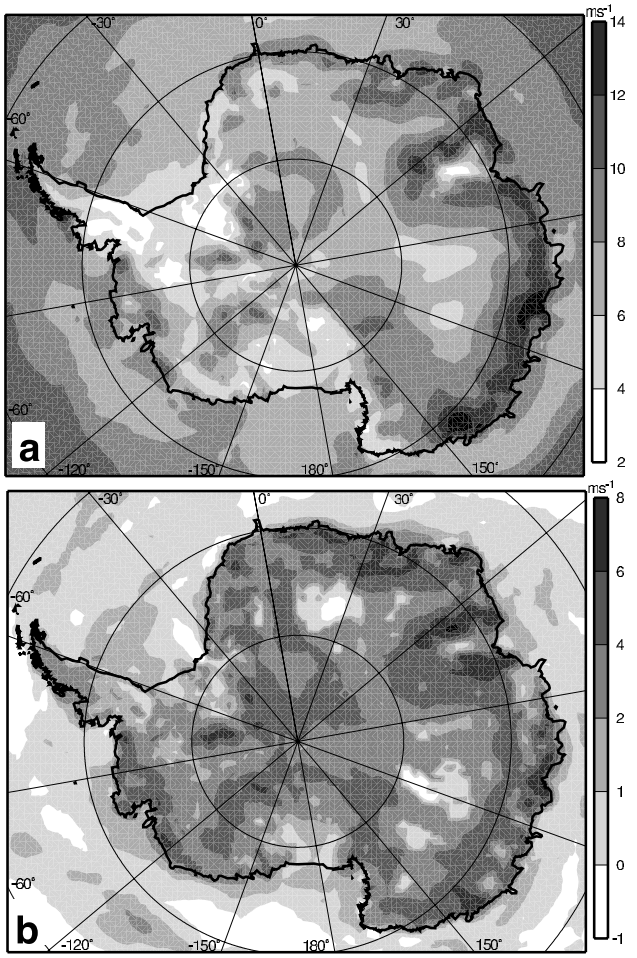

Figure 4. Monthly averaged modeled 10-m wind speed in CTL (a) and the difference in 10-m wind speed with respect to ORI (CTL - ORI) (b) for July 1998.

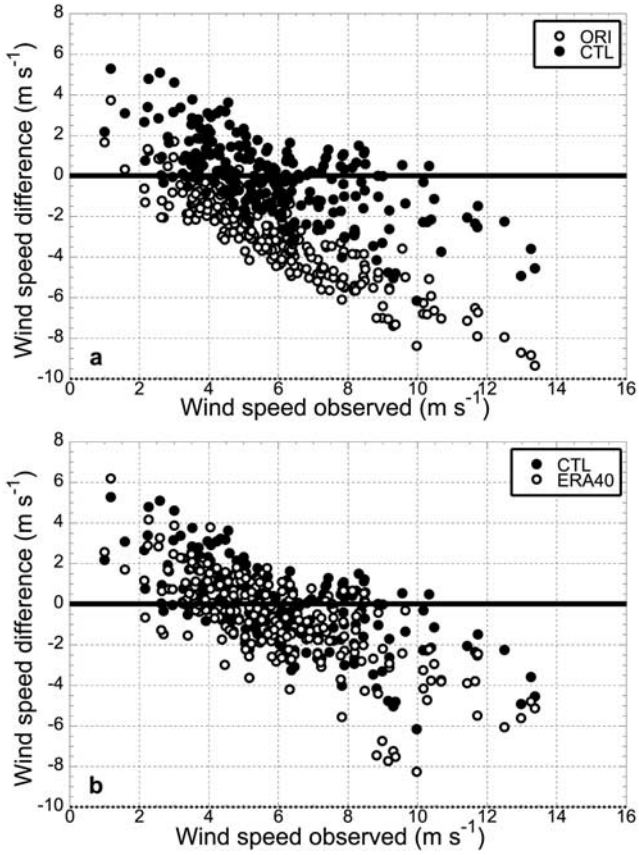

Figure 5. Monthly averaged 10-m wind speed differences (model - observations) as a function of the (automatic) weather station observations for experiments ORI and CTL (a), and in CTL and ERA40 (b) for 1998. Observations were recalculated to 10 m using a logarithmic vertical wind profile.

Table 4. Comparison of Modeled and Observed 10-m Wind Speed (*WS*) and 2-m Temperature (T_2)[a]

	T_2, K		*WS*, m s^{-1}	
	Bias	σ	Bias	σ
		January		
ORI	4.5	5.1	−2.1	2.6
CTL	0.8	2.2	−0.2	1.1
ERA40	5.4	6.1	−0.2	1.4
		July		
ORI	−2.5	4.9	−3.3	4.3
CTL	−2.3	3.9	0.1	2.3
ERA40	2.7	4.0	−0.5	2.8
		1998		
ORI	1.7	4.2	−3.1	3.8
CTL	−0.7	3.4	−0.1	1.9
ERA40	3.5	4.5	−0.7	2.3

[a]Averages over all surface stations are presented, and are monthly averages for January and July 1998, and annual averages for 1998. Bias is the average difference (model - observations); σ is the standard deviation of the difference over all stations.

Figure 6a and Table 4 show that the bias is largest in ORI in winter (∼−3.3 m s^{-1}), while in CTL the bias is about ±0.3 m s^{-1} year-round.

[33] Figure 7a presents an example of the diurnal cycle in wind speed (modeled and observed) at AWS 2, a site in the escarpment region of East Antarctica. The diurnal cycle in wind speed is the result of diurnal variations in the katabatic forcing which results in a maximum in wind speed in early morning. Because it is mainly a feature of the katabatic flow, the diurnal cycle is most pronounced in the escarpment region. In the model, the diurnal cycle is underestimated or not even present, and when present CTL is slightly better in reproducing it than ORI. The limited horizontal resolution of the model is partly responsible for the underestimation of the diurnal cycle.

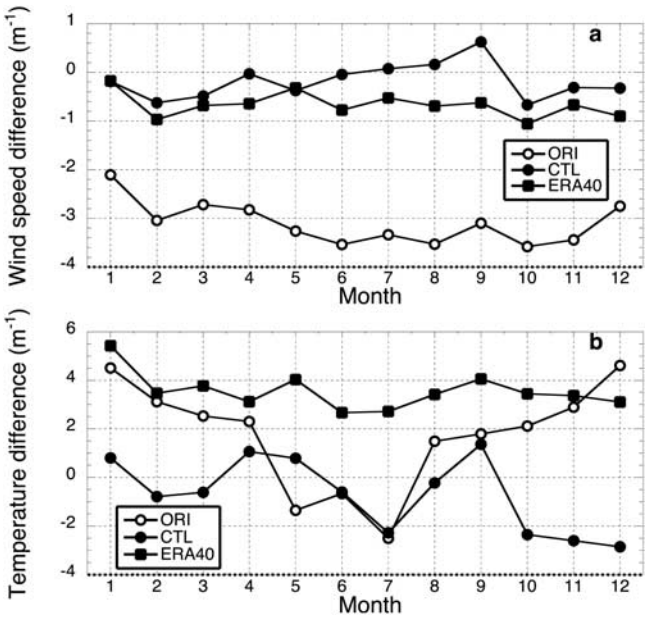

Figure 6. Monthly averaged (a) 10-m wind speed and (b) 2-m temperature differences (model - observations) averaged over all (automatic) weather station sites as a function of time of year. Wind speed observations were recalculated to 10 m using a logarithmic vertical wind profile.

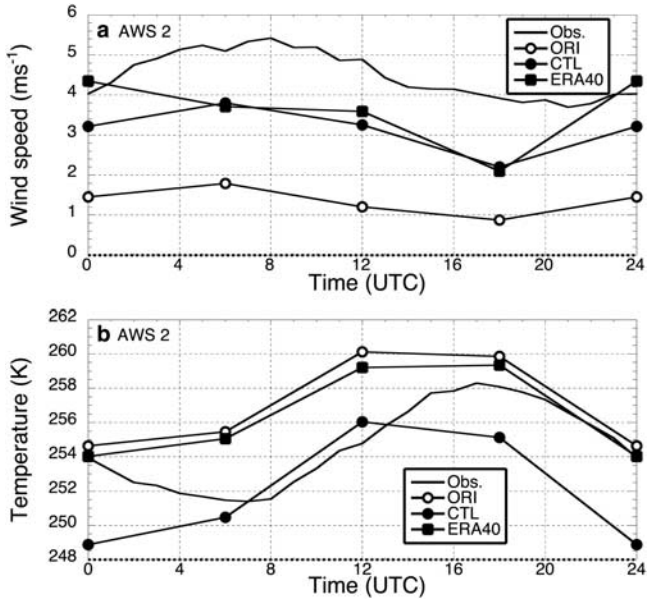

Figure 7. Average modeled and observed diurnal cycle of (a) wind speed and (b) temperature at AWS 2 for January 1998. AWS 2 is an automatic weather station in the escarpment region of East Antarctica (Figure 1).

3.1.2. Temperature

[34] Table 3 presents the temporal and continentally averaged near-surface temperatures for January, July and the year 1998. The modeled 2-m temperature is based on interpolation between the skin temperature and the temperature of the lowest model level using the profile functions of the parameterization of the surface fluxes. Figure 8a shows that the model generally overestimates the 2-m temperature. The modeled 2-m temperature improves significantly in CTL, especially in summer (Figure 6b and Table 4). The 2-m temperature is not very sensitive to changes in the initial snow temperature owing to the use of a skin layer formulation (not shown). The improvement in CTL is mainly due to an albedo change; α_{min} was increased and equation (3) was introduced (Table 1). Both albedo changes increase the snow albedo. As a result, the amount of energy available for heating the surface reduces, and the near-surface temperatures decrease. The effect is largest in summer and for the sites on the Antarctic plateau where cloud amounts are low, insolation is high and temperatures are low (Figure 9). Averaged over the continent the reduction in temperature from ORI to CTL is ∼5°C in summer and ∼3°C annually (Table 3). With the introduction of the model changes the diurnal cycle in temperature in summer improves in shape of the cycle as well as in absolute value. Figure 7b presents, as an example, the diurnal cycle in temperature at AWS 2 in January.

3.2. Vertical Profiles

[35] The proposed changes to the model physics all describe changes in surface properties. However, the effect of such changes is not confined to the boundary layer [*Beljaars and Viterbo*, 1998; *Reijmer et al.*, 2004]. In atmospheric models the main impact of the (stable) bound-

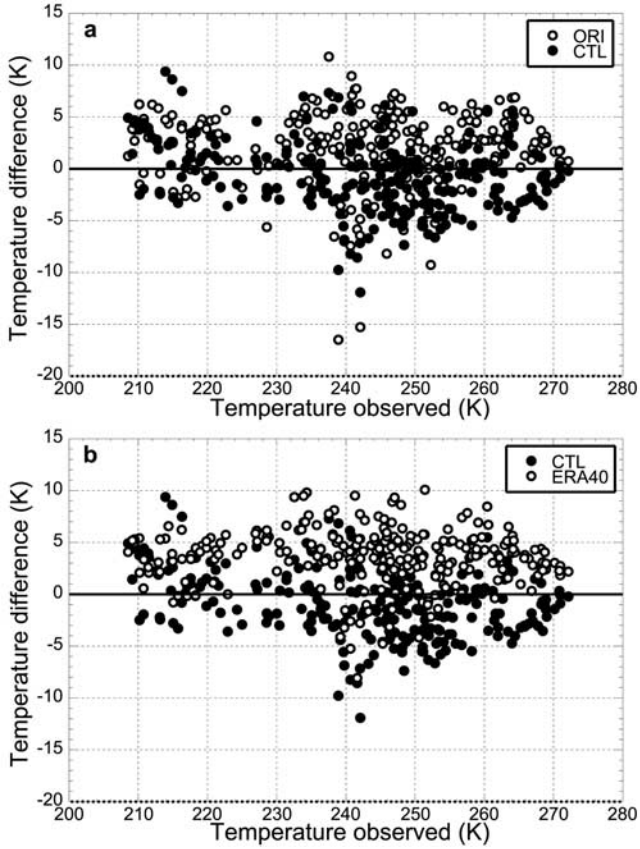

Figure 8. Monthly averaged 2-m temperature differences (model - observations) as a function of (automatic) weather station observations for experiments (a) ORI and CTL and (b) CTL and ERA40 for 1998.

ary layer on the rest of the atmosphere is through the surface fluxes by way of vertical diffusion. Here, we describe the effect of the proposed changes on the vertical profiles of wind, temperature and specific humidity.

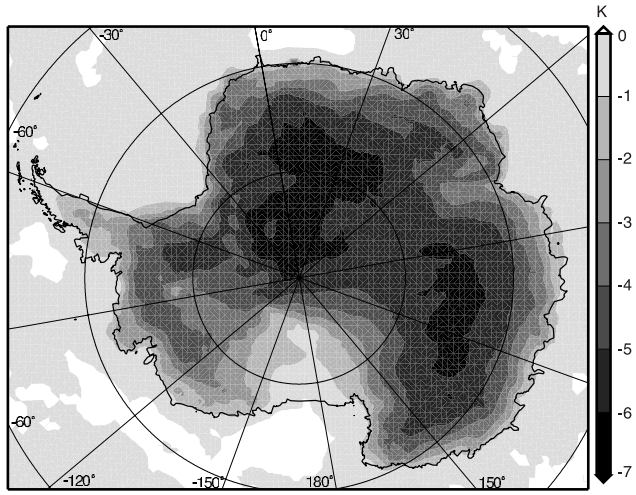

Figure 9. Monthly averaged modeled 2-m temperature difference between CTL and ORI (CTL - ORI) for January 1998.

3.2.1. Wind Speed

[36] Wind speed changes originating from changes in the surface formulation are not restricted to the boundary layer. Figure 10 presents the annual and continentally averaged zonal and meridional components of the wind in ORI and CTL. Due to the decrease in z_{0m}, the wind speed increases over the total atmospheric column. The increase is largest in the zonal component, near the surface and in winter. The annual averaged wind speed increases by $\sim$3.4 m s^{-1} near the surface (Table 3), and by $\sim$0.5 m s^{-1} above the boundary layer. The layer where the wind has an easterly component thickens on average by $\sim$80 hPa and the surface layer shows a more pronounced katabatic jet in CTL throughout the year.

[37] Figure 11 presents the monthly averaged profiles for the zonal and meridional components of the wind for Neumayer and South Pole, for January and July 1998. In both months and at both locations the shape of the modeled profiles for wind speed is reasonable for both experiments (not shown). In January, the wind speed is underestimated by 1 to 2 m s^{-1} throughout the troposphere. In ORI the underestimation is larger near the surface. In July the modeled wind speed above the boundary layer is higher resulting in an overestimation of $\sim$1 m s^{-1} in ORI and a small underestimation of $\sim$0.5 m s^{-1} in CTL. At both locations the general shape of vertical profiles of the wind components is reasonably well reproduced by the model. At Neumayer, discrepancies are largest in the zonal component in ORI, and near the surface. Furthermore, the layer with a southern component is much thinner in the observations than in both model experiments. At South Pole, the zonal component is best reproduced in ORI while the meridional component is best reproduced in CTL (Table 5). At both

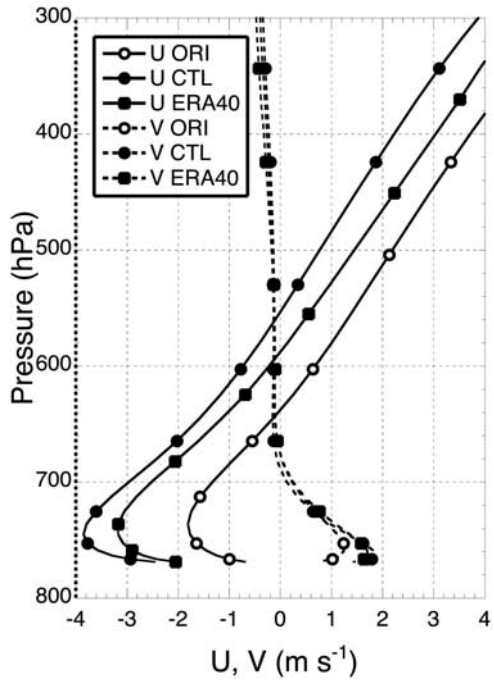

Figure 10. Annual and continentally averaged modeled profiles of the zonal (U) and meridional (V) wind speed components for 1998.

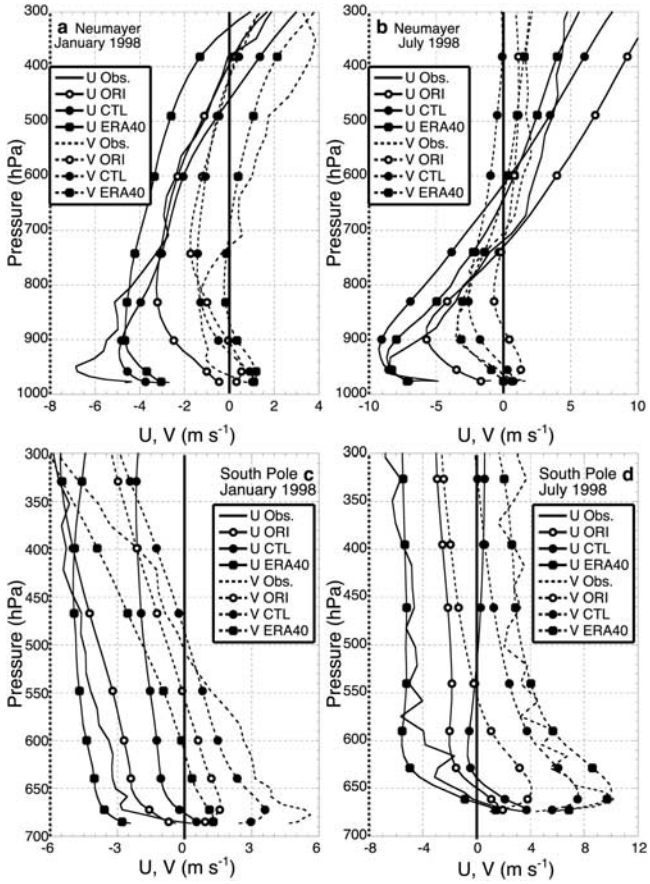

Figure 11. Monthly averaged modeled and observed profiles of the zonal (U) and meridional (V) wind speed components at (a, b) Neumayer and (c, d) South Pole for (a, c) January and (b, d) July 1998. At South Pole the U component is defined positive along the 0° meridian, and the V component is defined positive along the 90°E meridian.

locations the wind profiles are slightly better after the inclusion of the changes to the model formulation.

3.2.2. Temperature

[38] In stable boundary layers the main impact of changes at the surface on the conditions above the boundary-layer is through the momentum flux. Changes in temperature are confined to the lower troposphere. Since the changes in the physics all impact at the surface, the continent averaged temperature change is largest at the surface with an average decrease of 0.5°C in winter to 4.5°C in summer (~3°C annually). In summer, the differences decrease to less than ±0.5°C above 1000 to 1500 m altitude (~150 hPa above the surface, Figure 12a). In winter, the model changes result in an increase in temperature above the surface layer. This difference is due to the fact that in summer the change in albedo dominates the changes in the temperature profile while in winter, the change in roughness length is most important. Due to the decrease in roughness length for momentum, wind speeds increase, enhancing mixing of relatively warm air from above the boundary layer into the layer, which results in an increase in temperature. Annually, the proposed changes decrease the average boundary-layer temperature.

[39] The average surface based temperature inversion, defined as the temperature difference between the surface and the maximum temperature in the lowest km, increases on average with ~2°C when introducing the model changes (ORI to CTL). In January the height of the maximum increases while in July it decreases. Annually, the height of the maximum remains at about the same height. The temperature lapse rate in the free atmosphere does not change significantly throughout the year.

[40] At individual sites, temperature differences between the experiments are in the order of ±2°C in January, except near the surface where differences up to ~4°C occur (Figure 13). In July, the differences are larger, up to ~5°C. Both at Neumayer and South Pole, near-surface temperatures in ORI are too high in January and too low in July. In CTL they correspond better to the observations. In absolute sense the temperature lapse rate is too large at both locations in both experiments. Differences between the experiments are largest near the surface and are, as for the near-surface temperatures, mainly caused by albedo changes in summer and increased wind speed due to the decreased roughness length in winter. The changes in the albedo have a cooling effect on the complete temperature profile while the increased wind speeds have a warming effect in the boundary layer. The change in albedo is also responsible for the appearance of a surface temperature inversion in CTL in summer at both locations. In terms of profile averaged bias and standard deviation the changes in model formulation improve the results (Table 5).

[41] Since temperature is the main limiting factor of Antarctic atmospheric moisture content, the modeled specific humidity profiles follow temperature (Figure 12b). Compared to observations the model performs reasonable

Table 5. Comparison Between Monthly Averaged Modeled and Observed Profiles of Temperature (*T*), Specific Humidity (*q*), Zonal (*U*), and Meridional (*V*) Component of the Wind, and Wind Speed (*WS*) for Neumayer and South Pole for January and July 1998[a]

	T, K		*q*, g kg^{-1}		*U*, m s^{-1}		*V*, m s^{-1}		*WS*, m s^{-1}	
	Bias	σ	Bias	σ	Bias	σ	Bias	σ	Bias	σ
Neumayer, January										
ORI	0.3	1.3	0.19	0.30	1.7	2.8	−0.9	1.8	−2.1	2.6
CTL	−0.8	1.0	0.02	0.07	0.9	1.1	−0.9	1.8	−1.3	1.4
ERA40	0.4	1.2	0.08	0.13	0.1	1.5	0.3	1.1	−0.6	0.7
Neumayer, July										
ORI	−2.7	3.0	−0.11	0.15	3.0	3.9	0.5	1.8	0.2	2.1
CTL	−2.1	2.4	−0.09	0.12	−0.7	2.5	−0.9	1.7	0.3	1.0
ERA40	0.7	1.5	0.02	0.06	−0.8	1.3	−0.5	0.7	0.1	0.8
South Pole, January										
ORI	2.1	3.7	0.30	0.41	0.5	0.7	−1.2	2.4	−1.7	2.3
CTL	1.0	1.9	0.23	0.30	2.5	2.7	−0.1	1.5	−1.7	1.8
ERA40	4.0	5.3	0.34	0.46	−0.4	1.2	−2.3	2.7	−1.1	1.3
South Pole, July										
ORI	−3.4	3.8	0.01	0.02	2.0	2.5	−4.4	4.6	−2.2	3.0
CTL	−1.9	2.6	0.02	0.02	4.2	4.7	−1.5	1.9	−0.8	1.4
ERA40	−2.3	2.8	0.01	0.02	−0.6	1.2	0.3	1.3	−0.4	1.4

[a]Bias is the profile averaged difference (model - observations); σ is the standard deviation of the difference. At South Pole the U component is defined positive along the 0° meridian, and the V component is defined positive along the 90°E meridian.

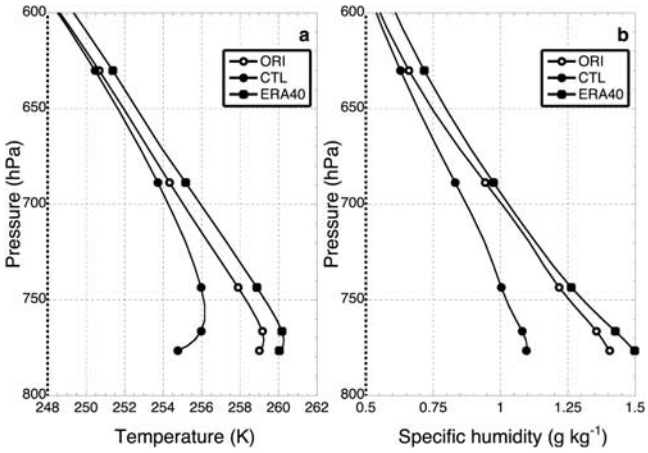

Figure 12. Monthly and continentally averaged modeled (a) temperature and (b) specific humidity profiles for January 1998.

in summer and underestimates moisture content in winter (Figures 13b and 13d). Discrepancies are largest at South Pole (not shown). However, this need not be a model deficiency. Observing humidity is difficult at low temperatures. In addition, the relatively large response times of the radiosondes used for the profile observations, and the fact that they are prepared indoors could explain the large discrepancy between modeled and observed humidity [*Hudson et al.*, 2004]. The large response times could also affect the temperature observations.

4. Results: Model Intercomparison

[42] In this section we compare the results of the 1998 CTL run with results from the ERA40 reanalysis for 1998.

4.1. Near-Surface Conditions

4.1.1. Wind Speed

[43] The overestimated low wind speeds and underestimated high wind speeds as found in CTL are found also in ERA40 (Figure 5b). It is likely that this is a general characteristic of Antarctic atmospheric models; it is a result of the katabatic nature of the near-surface wind over Antarctica in combination with the smoothing of the topography. In ERA40 the wind speeds are on average lower than in CTL (Table 3), resulting in a more negative bias between modeled and observed wind speed compared to CTL (Figure 6 and Table 4). The spread in the values is also larger, resulting in higher values of the standard deviation of the difference. In addition, ERA40 has, for the same reasons as CTL, problems reproducing the diurnal cycle in wind speed in summer (Figure 7a). These problems in ERA40 are surprising because the ERA40 values are based on analyses in which (profile) observations are incorporated. On the other hand, the orography used in ERA40 is less accurate than the one used in RACMO2/ANT, z_{0m} is clearly overestimated, and the resolution is coarser.

[44] Averaged over the continent, wind speeds in ERA40 are up to 1.0 m s^{-1} lower than in CTL. The largest differences between ERA40 and CTL are found in the escarpment region (Figure 14) where differences in z_{0m} are largest. This suggests that the lower wind speeds in ERA40 are mainly due to a larger z_{0m}. Over the plateau wind speeds in ERA40 are slightly higher compared to CTL. The differences are most pronounced in winter. This could be explained by higher surface temperatures in ERA40 (see next section) resulting in less stable conditions, especially over the higher plateau in winter.

4.1.2. Temperature

[45] Figure 8b and Table 4 present the results of the comparison between observed temperature and the two different models. Generally, the near-surface temperature is best modeled by CTL, especially for the summer months. An exception to this is the northern part of the Antarctic Peninsula where winter temperatures are too low in CTL (not shown). This is due to the way sea ice is prescribed, in which fractional sea ice cover is not allowed for. ERA40 allows for fractional sea ice cover. As a result, in winter, when the sea is only partially covered by ice in this area, the model overestimates the sea ice cover resulting in too low temperatures.

[46] ERA40 suffers from an overestimation of the near-surface temperature in the summer months likely because of a too low surface albedo (Figure 6b). In ERA40 the snow albedo is described by equations (1) and (2) and is often close to 0.75. ERA40 has the same problem in reproducing the diurnal cycle in temperature in summer as ORI (Figure 7b), which is due to the low surface albedo of

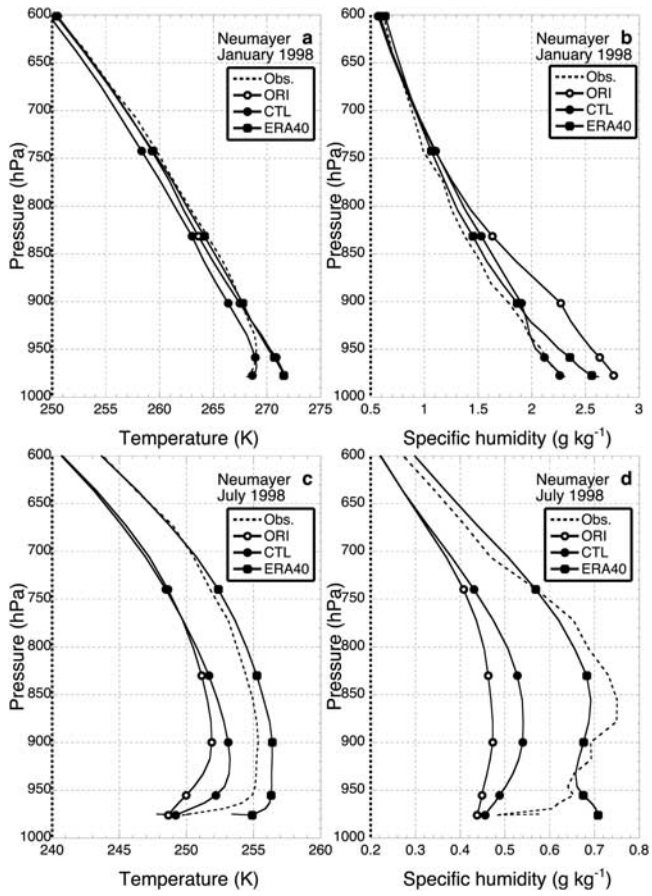

Figure 13. Monthly averaged modeled and observed profiles of (a, c) temperature and (b, d) specific humidity at Neumayer for January and July 1998.

ERA40 and the resulting less stable conditions in the boundary layer. ERA40 is also in winter generally too warm. This is not unexpected because the operational ECMWF model also experiences a warm bias in winter. This warm bias is often ascribed to the used exchange coefficients in the ECMWF model. To prevent decoupling of the surface from the lowest model levels under very stable conditions they were changed to enhance heat exchange under these conditions [*Viterbo et al.*, 1999]. However, RACMO2/ANT uses the same physics parameterizations for the turbulent fluxes as used in ERA40 and CTL does not show such a warm bias in winter. An explanation could be that mixing in ERA40 is enhanced due to the overestimation of z_{0m}, or that the surplus in heat stored in the snow surface in summer is large enough to increase the near-surface temperature throughout the winter.

[47] Continental averaged temperature shows the same pattern with higher temperatures in ERA40 throughout the year (Table 3). In summer, the differences between CTL and ERA40 can be as large as 10°C on the high Antarctic plateau where cloud amounts are low, insolation is high, the albedo is high and accumulation is low (Figure 15). In winter differences are generally smaller. In ERA40, temperature is relatively high over the large ice shelves and sea ice which can be explained by the lower surface albedo in ERA40 and the partial sea ice cover possible in ERA40.

4.2. Vertical Profiles

4.2.1. Wind Speed

[48] The wind profiles in ERA40 correspond better to measurements than the CTL profiles (Table 5 and Figure 11). This is likely due to the fact that in ERA40 analyses almost all observed profiles are incorporated. Therefore, ERA40 data are not independent of the observations. Figure 11 presents, as an example, the monthly averaged modeled and observed zonal and meridional wind components at Neumayer and South Pole for January and July 1998. CTL generally captures the shape of the profiles but underestimates wind speed by an almost constant value of 1–2 m s^{-1} while ERA40 remains within ±0.5 m s^{-1}, except near the surface where ERA40 underestimates wind speeds up to 2 m s^{-1}.

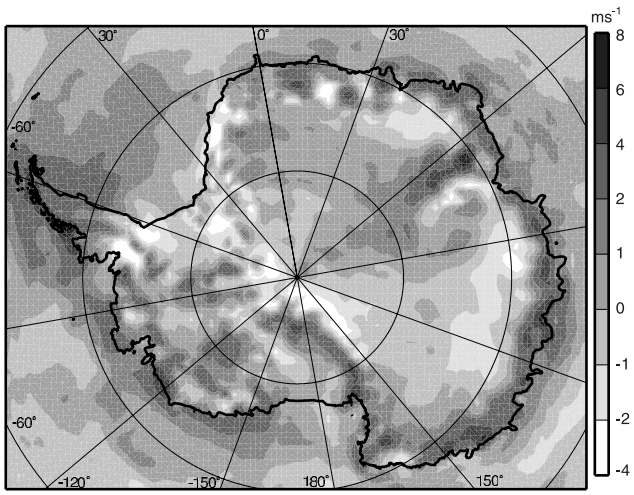

Figure 14. Monthly averaged modeled 10-m wind speed difference between CTL and ERA40 for July 1998 (CTL - ERA40).

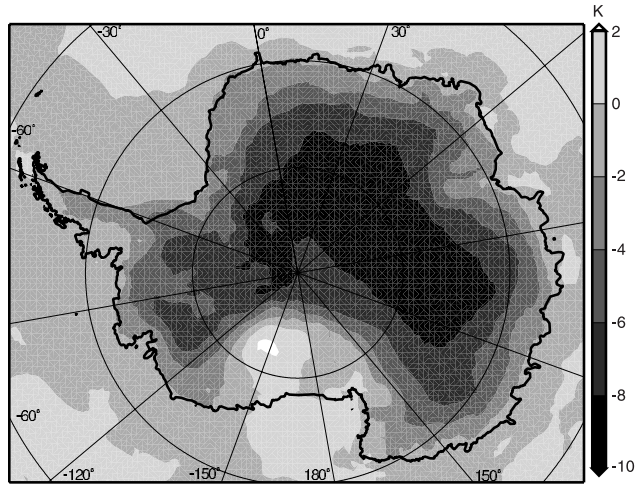

Figure 15. Monthly averaged modeled 2-m temperature difference between CTL and ERA40 for January 1998 (CTL - ERA40).

4.2.2. Temperature

[49] For temperature and specific humidity the largest differences between the models and the largest discrepancy between models and observations occurs close to the surface and disappears at higher altitudes (Figure 13). Temperature and humidity are also best reproduced by ERA40 although differences are small. The correspondence between ERA40 and observations is best at higher altitudes. Near the surface, ERA40 overestimates the temperature in summer as well as in winter. This overestimation is largest at South Pole, on the Antarctic plateau.

[50] Specific humidity follows, as expected, temperature. Therefore, because temperatures are too high in ERA40, the moisture content is also too high. Note, however, that observing moisture content at low temperatures is problematic.

5. Summary and Conclusions

[51] We used a regional atmospheric climate model (RACMO2/ANT) to simulate the atmosphere over Antarctica. We adapted the model to better represent the specific conditions over the Antarctic continent and tested the changes by comparing changed and unchanged model results with observations. The changes to the model formulation are clearly improving the model performance near the surface. Wind speed is mostly improved by reducing the surface roughness length for momentum. Temperature and humidity are improved by increasing the snow albedo. Comparison with observed vertical profiles at Neumayer and South Pole, locations representative for the coastal area and Antarctic plateau, show that the model changes on average reduce temperature, specific humidity and wind speed throughout the entire column, which is a small improvement.

[52] Compared to ERA40, RACMO2/ANT performs reasonably well, especially near the surface. The near-surface temperature corresponds better to observations compared to ERA40 due to a higher surface albedo. The near-surface wind speed corresponds best to the observations because of

the lower roughness length for momentum. In terms of vertical profiles best correspondence is found in ERA40 owing to the fact that the observed profiles are incorporated in the analyses used for the comparison. The model results are therefore not independent of the observations, but again, near the surface RACMO2/ANT performs better than ERA40. This is mainly because of the overestimation of the near-surface temperature and wind speed in ERA40.

[53] The fact that the comparison with observations gives reasonable to good results for RACMO2/ANT is encouraging, especially since the model is operated in climate mode, i.e., it is initialized once and thereafter only forced at the lateral boundaries. The results presented here show that RACMO2/ANT contains additional value over ERA40. Therefore a climate run with RACMO2/ANT was carried out for a 45-year period using ERA40 at its boundaries. The results are presented by *Van de Berg et al.* [2005] and forthcoming papers.

[54] **Acknowledgment.** Financial support was provided by the Netherlands Antarctic Research Programme (ALW), which is part of the Netherlands Organization of Scientific Research (NWO).

References

Andreas, E. L. (1987), A theory for the scalar roughness and the scalar transfer coefficients over snow and sea ice, *Boundary Layer Meteorol.*, *38*(1–2), 159–184.

Andreas, E. L. (2002), Parameterizing scalar transfer over snow and ice: A review, *J. Hydrometeorol.*, *3*, 417–432.

Beljaars, A. C. M., and P. Viterbo (1998), Role of the boundary layer in a numerical weather prediction model, in *Clear and Cloudy Boundary Layers*, pp. 287–304, R. Neth. Acad. of Arts and Sci., Amsterdam.

Bintanja, R. (2000), Surface heat budget of Antarctic snow and blue ice: Interpretation of spatial and temporal variability, *J. Geophys. Res.*, *105*(D19), 24,387–24,407.

Bromwich, D. H., A. J. Monaghan, and Z. Guo (2004), Modeling the ENSO modulation of Antarctic climate in the late 1990s with the polar MM5, *J. Clim.*, *17*, 109–132.

Cassano, J. J., T. R. Parish, and J. C. King (2001), Evaluation of turbulent surface flux parameterizations for the stable surface layer over Halley, Antarctica, *Mon. Weather Rev.*, *129*, 26–46.

Cullather, R., D. Bromwich, and M. van Woert (1996), Interannual variations in Antarctic precipitation related to El Nino-Southern Oscillation, *J. Geophys. Res.*, *101*(D14), 19,109–19,118.

Cullather, R., D. Bromwich, and M. van Woert (1998), Spatial and temporal variability of Antarctic precipitation from atmospheric methods, *J. Clim.*, *11*, 334–367.

Douville, H., J.-F. Royer, and J.-F. Mahfouf (1995), A new snow parameterization for the Meteo-France climate model. Part I: Validation in standalone experiments, *Clim. Dyn.*, *12*, 21–35.

Fouquart, Y., and B. Bonnel (1980), Computations of solar heating of the earth's atmosphere: A new parameterization, *Contrib. Atmos. Phys.*, *53*, 35–62.

Genthon, C., and A. Braun (1995), ECMWF analysis and predictions of the surface climate of Greenland and Antarctica, *J. Clim.*, *8*, 2324–2332.

Gibson, J. K., P. Kållberg, S. Uppala, A. Hernandez, A. Nomura, and E. Serrano (1997), ERA-15 description, *ECMWF Reanaly. Proj. Rep. Ser. 1*, 72 pp., Eur. Cent. for Medium-Range Weather Forecasts, Reading, England.

Guo, Z., D. H. Bromwich, and J. Cassano (2003), Evaluation of polar MM5 simulations of Antarctic atmospheric circulation, *Mon. Weather Rev.*, *131*, 384–411.

Hines, K. M., D. H. Bromwich, and G. J. Marshall (2000), Artificial surface pressure trends in the NCEP-NCAR reanalysis over the Southern Ocean and Antarctica, *J. Clim.*, *13*, 3940–3952.

Hudson, S. R., M. S. Town, V. P. Walden, and S. G. Warren (2004), Temperature, humidity and pressure response of radiosondes at low temperatures, *J. Atmos. Oceanic Technol.*, *21*, 825–836.

King, J. C., and J. Turner (1997), *Antarctic Meteorology and Climatology*, 409 pp., Cambridge Univ. Press, New York.

King, J. C., W. Connelley, and S. Derbyshire (2001), Sensitivity of modelled Antarctic climate to surface and boundary layer flux parameterisations, *Q. J. R. Meteorol. Soc.*, *127*, 779–794.

König-Langlo, G. C., J. C. King, and P. Pettre (1998), Climatology of the three coastal Antarctic stations Dumont d'Urville, Neumayer, and Halley, *J. Geophys. Res.*, *103*(D9), 10,935–10,946.

Louis, J. F. (1979), A parametric model of vertical eddy fluxes in the atmosphere, *Boundary Layer Meteorol.*, *17*, 187–202.

Mlawer, E. J., S. J. Taubman, P. D. Brown, M. J. Iacono, and S. A. Clough (1997), Radiative transfer for inhomogeneous atmospheres: RRTM, a validated correlated-k model for the longwave, *J. Geophys. Res.*, *102*(D2), 16,663–16,682.

Parish, T. R., and D. H. Bromwich (1991), Continental-scale simulation of the Antarctic katabatic wind regime, *J. Clim.*, *4*, 135–146.

Reijmer, C. H., and J. Oerlemans (2002), Temporal and spatial variability of the surface energy balance in Dronning Maud Land, Antarctica, *J. Geophys. Res.*, *107*(D24), 4759, doi:10.1029/2000JD000110.

Reijmer, C. H., E. van Meijgaard, and M. van den Broeke (2004), Numerical studies with a regional atmospheric climate model based on changes in the roughness length for momentum and heat over Antarctica, *Boundary Layer Meteorol.*, *111*, 313–337.

Reusch, D. B., and R. B. Alley (2004), A 15-year West Antarctic climatology from six automatic weather station temperature and pressure records, *J. Geophys. Res.*, *109*, D04103, doi:10.1029/2003JD004178.

Stearns, C. R., R. E. Holmes, and G. A. Weidner (1997), Antarctic automatic weather stations: 1996–1997, *Antarct. J. U. S.*, *32*(5), 174–178.

Tiedke, M. (1989), A comprehensive mass flux scheme for cumulus parameterization in large-scale models, *Mon. Weather Rev.*, *117*, 1779–1800.

Troen, I., and L. Mahrt (1986), A simple model of the atmospheric boundary layer; sensitivity to surface evaporation, *Boundary Layer Meteorol.*, *37*, 129–148.

Turner, J., W. M. Connelley, S. Leonard, G. J. Marshall, and D. G. Vaughan (1999), Spatial and temporal variability of net snow accumulation over the Antarctic from ECMWF reanalysis project data, *Int. J. Climatol.*, *19*, 697–724.

Undén, P., et al. (2002), The high resolution limited area model, in *Hirlam-5 Scientific Documentation*, 144 pp., Swed. Meteorol. Hydrol. Inst., Norrköping, Sweden.

Van As, D., et al. (2005), The summertime energy balance on the high Antarctic plateau, *Boundary Layer Meteorol.*, in press.

Van de Berg, W. J., et al. (2005), Characteristics of the Antarctic surface mass balance (1958–2002) using a regional atmospheric climate model, *Ann. Glaciol.*, in press.

Van den Broeke, M. R. (2000), On the interpretation of Antarctic temperature trends, *J. Clim.*, *31*, 3885–3889.

Van den Broeke, M. R., N. P. M. van Lipzig, and E. van Meijgaard (2002), Momentum budget of the East-Antarctic atmospheric boundary layer: Results of a regional climate model, *J. Atmos. Sci.*, *59*, 3117–3129.

Van den Hurk, B., and P. Viterbo (2003), The torne-kalix PILPS 2(e) experiment as a test bed for modifications to the ECMWF land surface scheme, *Global Planet. Change*, *38*, 165–173.

Van Lipzig, N. P. M. (1999), The surface mass balance of the antarctic ice sheet, Ph.D. thesis, 154 pp., Inst. for Mar. and Atmos. Res., Utrecht Univ., Utrecht, Netherlands.

Van Lipzig, N. P. M., E. van Meijgaard, and J. Oerlemans (1999), Evaluation of a regional atmospheric model using measurements of surface heat exchange processes from a site in Antarctica, *Mon. Weather Rev.*, *127*, 11,994–12,011.

Van Lipzig, N. P. M., E. van Meijgaard, and J. Oerlemans (2002), The spatial and temporal variability of the surface mass balance in Antarctica: Results from a regional climate model, *Int. J. Climatol.*, *22*, 1197–1217.

Viterbo, P., A. Beljaars, J.-F. Mahfouf, and J. Teixeira (1999), The representation of soil moisture freezing and its impact on the stable boundary layer, *Q. J. R. Meteorol. Soc.*, *125*, 2401–2426.

Walsh, K., and J. L. McGregor (1996), Simulations of the Antarctic climate using a limited area model, *J. Geophys. Res.*, *101*(D14), 19,093–19,108.

Warren, S. G. (1982), Optical properties of snow, *Rev. Geophys.*, *20*(1), 67–89.

White, P. W. (2001), Part IV: Physical processes (CY23R4), technical report, 101 pp., Eur. Cent. for Medium-Range Weather Forecasts, Reading, England.

C. H. Reijmer and M. R. van den Broeke, Institute for Marine and Atmospheric Research, Utrecht University, Princetonplein 5, 3584 CC Utrecht, Netherlands. (c.h.tijm-reijmer@phys.uu.nl)

E. van Meijgaard, Royal Netherlands Meteorological Institute, 3730 AE De Bilt, Netherlands.